COMPARISON OF DNS OF COMPRESSIBLE AND INCOMPRESSIBLE TURBULENT DROPLET-LADEN HEATED CHANNEL FLOW WITH PHASE TRANSITION

A. Bukhvostova[1], *E. Russo*[2], *J.G.M. Kuerten*[2,1] *and B.J. Geurts*[1,3]

[1] *Faculty EEMCS, University of Twente, Enschede, NL*
[2] *Department of Mechanical Engineering, Eindhoven University of Technology, NL*
[3] *Department of Technical Physics, Eindhoven University of Technology, NL*

a.bukhvostova@utwente.nl

Abstract

In this paper a turbulent channel flow with dispersed droplets is examined. The dispersed phase is allowed to have phase transition, which leads to heat and mass transfer between the phases, and correspondingly modulates turbulent flow properties. As a point of reference we examine the flow of water droplets in air, containing also the vapor of water. The key element of this study concerns the treatment of the carrier phase as either a compressible or an incompressible fluid. We compare simulation results obtained with a pseudo-spectral discretization for the incompressible flow to those obtained with a finite volume approach for the compressible flow. The compressible formulation is not tailored for low Mach flow and we need to resort to a Mach number that is artificially high for simulation feasibility. We discuss differences in fluid flow, heat- and mass transfer and dispersed droplet properties. The main conclusion is that both formulations give a good general correspondence. Flow properties such as velocity fields agree very closely, while heat transfer as characterized by the Nusselt number differs by around 25%. Droplet sizes are shown to be slightly larger, particularly in the center of the channel, in case the compressible formulation is chosen. A low-Mach compressible formulation is required for a fully quantitative comparison.

1 Introduction

Multiphase flows with a large number of droplets dispersed into a gas play an important role in a variety of technological applications. Examples include thermal processing in food manufacturing, air pollution control and heat transfer in power stations. In this paper we investigate a coupled Euler-Lagrange model to simulate particle-laden turbulent channel flow in which phase transition plays an important role.

The dispersed phase exhibits not only momentum exchange with the carrier phase but, in addition, contributes to the character of the turbulent flow by phase transition, which adds energy and mass transfer between the carrier phase and the discrete droplets. Not so many studies focus on mass and heat transfer in droplet-laden turbulent channel flow. Mashayek (1997) made the first Euler-Lagrange simulation study, investigating homogenous turbulence with two-way coupling in momentum, mass and heat transfer. In this paper we extend this work by investigating inhomogeneous turbulent channel flow with a dispersed droplet phase undergoing phase transition.

We study a heated droplet-laden channel flow in which the top wall is heated uniformly and the bottom wall is cooled. As a point of reference we consider the flow of droplets of water in air, in which the presence of water vapor is accounted for. The mixture of air and water vapor will be referred to as the carrier phase and liquid droplets as the dispersed phase.

Proper incorporation of evaporation and condensation of the dispersed phase raises the question whether or not to include explicit compressibility of the carrier phase. If the carrier gas is assumed to be strictly incompressible then the inclusion of evaporation and condensation is subject to the condition that all instantaneous changes in the local mass density of air and water vapor cancel each other precisely throughout the domain. A full simulation model can be developed for such an incompressible carrier phase (Russo et al. (2011)). Here, we complement the incompressible model by a fully compressible description, which allows to quantify the consequences of non-constant mass density of the carrier phase and indicate in which respects the full compressible formulation becomes essential.

In the current compressible formulation the Mach number needs to be set artificially high in view of simulation efficiency. Since we do not employ a tailored low-Mach formulation, the use of realistic Mach numbers would imply time steps that are too low to yield affordable simulation times. Instead, we select a low, but nevertheless much larger Mach number. This is an important source of differences between the incompressible and compressible formulations, as will be discussed in Section 3. Generally, fluid flow, heat and

mass transfer properties are predicted in good agreement when comparing the compressible and incompressible formulations.

The organization of this paper is as follows. In Section 2 the mathematical model is formulated for the coupled droplets-carrier gas system. Simulation results comparing the incompressible and compressible models are presented in Section 3 and concluding remarks are collected in Section 4.

2 Mathematical formulation

In this section the full mathematical model, describing the coupled phases, will be presented. Moreover, the numerical method will be sketched. The incompressible results are used as point of reference, which are discussed in detail in Russo et al. (2011). Here, we will focus on the differences in mathematical formulation and numerical method.

Carrier phase equations

The carrier phase is composed of air and water vapor. It can be treated either as an incompressible or a compressible Newtonian fluid. The incompressible formulation in Russo et al. (2011) can be extended to include mass, momentum, energy and vapor density equations. The formulation of the governing equations as used here is close to Bird et al. (1960):

$$\partial_t \rho + \partial_j(\rho u_j) = Q_m \tag{1}$$
$$\partial_t(\rho u_i) + \partial_j(\rho u_i u_j) = -\partial_j \pi_{ij} + Q_{mom,i} \tag{2}$$
$$\partial_t e_t + \partial_j\left(\rho u_j e_t\right) = -\partial_j q_j - \partial_j(u_i \pi_{ij}) + Q_e \tag{3}$$
$$\partial_t(\rho Y_v) + \partial_j(\rho u_j Y_v) = -\partial_j J_{v,j} + Q_m \tag{4}$$

where $Q_m, Q_{mom,i}, Q_e$ are sink/source terms expressing the two-way coupling between the phases. These will be described momentarily. In this formulation (ρ, u_j, e_t, Y_v) are the carrier phase mass density, components of the velocity, total energy density and vapor mass fraction of the carrier phase, respectively. Moreover, π_{ij} defines pressure and viscous contributions to the momentum flux. We use Sutherlands's law to compute the dynamic viscosity. In addition, q_j denotes the components of the heat flux vector, which consists of heat transport by conduction and by diffusion. The vector J_v defines the diffusive mass flux of water vapor with respect to the mixture velocity. The pressure and temperature of the carrier phase are denoted by p and T and are connected by assuming the ideal gas law. In particular, each of the components in the carrier phase is treated as an ideal gas with a corresponding specific gas constant.

The equations (1)-(4) are made non-dimensional using a reference mass density, velocity, length and temperature. As the reference mass density ρ_{ref}, the initial mass density of the carrier is used at a pressure of 1 atm. The reference length L_{ref} is equal to 2 cm, denoting half the channel height. The Reynolds number is defined in the following way:

$$\mathrm{Re} = \frac{\rho_{ref}\, u_{ref}\, L_{ref}}{\mu_{ref}}$$

and will be specified further on. The reference velocity u_{ref} was found from the chosen Reynolds number and initial dynamic viscosity μ_{ref} of the carrier phase, which is known from setting the reference temperature to 293.15 K. In addition, the non-dimensional form of the governing equations contains the Prandtl and Mach numbers, which characterize the flow conditions.

Apart from the assumption that the flow is incompressible, $\partial_j u_j = 0$, the formulation by Russo et al. (2011) differs from the compressible formulation by adopting an equation for the gas temperature instead of an equation for the total energy density. Moreover, while an explicit equation of state is used to connect pressure and temperature in the compressible case, the incompressible formulation solves the pressure from a Poisson equation.

Comparing the present compressible model with the formulation used by Mashayek (1997), a close correspondence between the two systems of equations is apparent. The main difference is in the specific heats at constant volume of air and water vapor. While Mashayek (1997) treats these specific heats as equal, in this study this assumption is not made and consequently we derive a more complete expression for the internal energy density of the carrier phase:

$$e_{int} = (\rho - Y_v\rho)Tc_{vf} + Y_v\rho(\lambda + Tc_{vv}) \tag{5}$$

where c_{vf}, c_{vv}, λ are the values of the specific heats at constant volume of the carrier phase, of the vapor and latent heat, respectively. From (5) we can compute the temperature of the fluid.

Equations for droplet dynamics

In both the compressible and the incompressible formulation we use the same model for the dispersed phase. We assume that the droplets are spherical and we include evaporation and condensation. For the water-air system droplets are much heavier than the carrier fluid, and the Stokes drag force is dominant. Referring to the classification proposed by Elghobashi (1994), we focus on droplet volume fractions high enough so that two-way coupling is required, while the volume fraction is low enough for collisions between droplets to be negligible.

The droplets are tracked by solving their equations of motion. The location and velocity of individual droplets are governed by the kinematic condition:

$$\frac{d\,\mathbf{x}_i(t)}{dt} = \mathbf{v}_i \tag{6}$$

and Newton's law:

$$\frac{dm_i\mathbf{v}_i}{dt} = m_i\frac{\mathbf{u}\left(\mathbf{x}_i, t\right) - \mathbf{v}_i}{\tau_{d,i}}\left(1 + 0.15\mathrm{Re}_{d,i}^{0.687}\right) \tag{7}$$

where $m_i, \mathbf{v}_i$ are the mass and the velocity of droplet i, respectively, and $\mathbf{u}(\mathbf{x}_i, t)$ is the velocity of the fluid at the location $\mathbf{x}_i$ of the droplet. In addition, $\mathrm{Re}_{d,i}$ is the Reynolds number based on the diameter d_i of the droplet and $\tau_{d,i} = \rho_l d_i^2/(18\mu_f)$ denotes the droplet relaxation time. In this expression, ρ_l is the droplet mass density, and μ_f the dynamic viscosity of the fluid. Comparing with the equations for the dispersed phase proposed in Mashayek (1997), it can be seen that instead of solving the velocity equation for a single droplet, we use Newton's second law, equation (7), taking also into consideration changes in the droplet mass because of evaporation and condensation.

The temperature of a droplet can be derived from the first law of thermodynamics :

$$\frac{d}{dt}\left(m_i\, c_l\, T_i\right) = h_v \frac{dm_i}{dt} + h_m A_i \left(T_{g,i} - T_i\right) \quad (8)$$

where h_v in equation (8) denotes the enthalpy of vapor and contains latent heat and $T_{g,i}$ is the temperature of the carrier phase at the particle location $T_{g,i} = T(\mathbf{x}_i, t)$. Defining the enthalpy of water as $h_l = c_l T$, and the droplet volume by V_i, equation (8) can be written as:

$$\rho_l\, c_l\, \mathrm{V}_i \frac{dT_i}{dt} = \left(h_v - h_l\right) \frac{dm_i}{dt} + h_m A_i \left(T_{g,i} - T_i\right). \quad (9)$$

To close equation (9) we need expressions for dm_i/dt and h_m.

Applying the conservation of mass around a single spherical droplet (Russo et al. (2011)) the following equation for dm_i/dt can be derived:

$$\frac{dm_i}{dt} = -\frac{m_i\, \mathrm{Sh}}{3\,\tau_{d,i}\,\mathrm{Sc}} \ln\left(\frac{1 - Y_{v,\delta}}{1 - Y_{v,0}}\right) \quad (10)$$

where δ is the boundary layer thickness for the vapor concentration and $Y_{v,\delta}$ and $Y_{v,0}$ are the vapor mass fraction at δ and on the surface of the droplet, respectively. In addition, Sh denotes Sherwood number, and Sc Schmidt number, obtained from the correlation for a sphere $Sh = 2 + 0.6\mathrm{Re}_d^{1/2}\mathrm{Sc}^{1/3}$ (Bird (1960)). The driving quantity of (10) is the difference $Y_{v,\delta} - Y_{v,0}$, where $Y_{v,0}$ can be written in terms of the fluid temperature at the droplet location. In fact, the saturation pressure $p_{v,sat}$ can be calculated using Antoine's relation in terms of $T_{g,i}$. Subsequently, the ideal gas law can be used to calculate the vapor mass fraction at the surface of the droplet:

$$Y_{v,0} = \frac{p_{v,sat}(T_{g,i})}{T_{g,i} R_{water} \rho} \quad (11)$$

where R_{water} is the specific gas constant for water vapor. For forced convection around a sphere the following heat-transfer correlation is used, Bird (1960):

$$\frac{h_m\, d_i}{K_g} = 2 + 0.6\, \mathrm{Re}_d^{1/2}\, \mathrm{Pr}^{1/3} \quad (12)$$

where K_g is the thermal conductivity of the gas and Pr the Prandtl number. This completes the formulation for the droplet phase. What remains is the specification of the coupling between the carrier and the droplet phases.

Coupling terms

The governing equations for the carrier phase contain two-way coupling terms. These terms appear because of the mass, momentum and energy exchange between the carrier and the dispersed phases. The coupling terms are expressed as:

$$Q_{mass} = -\sum_i \frac{dm_i}{dt}\delta(\mathbf{x} - \mathbf{x}_i) \quad (13)$$

$$Q_{mom,j} = -\sum_i \frac{d}{dt}(m_i v_{i,j})\delta(\mathbf{x} - \mathbf{x}_i) \quad (14)$$

$$Q_e = -\sum_i \left(c_l \frac{d}{dt}(m_i T_i) + \frac{d}{dt}(\frac{1}{2} m_i v_{i,j}^2) \right) \delta(\mathbf{x} - \mathbf{x}_i) \quad (15)$$

where the sums are taken over all droplets in the domain. Coupling term (13) shows that mass transfer between the phases occurs because of evaporation and condensation of the droplets. Momentum transfer between the phases as expressed by (14), consists of two mechanisms: the drag force between the droplets and carrier gas and the momentum transfer due to mass transfer arising from the phase change. Finally, energy transfer occurs because of direct heat transfer between droplets and the carrier gas, because of changes in kinetic energy caused by the drag force and because of mass transfer by the phase change.

Numerical method and initial conditions

The incompressible and compressible models were simulated using different numerical methods. The incompressible formulation adopts the pseudo-spectral method for the carrier phase as described in Russo et al. (2011) and Kuerten (2006). The droplet equations are integrated in time with the same three-stage Runge-Kutta method as used for the nonlinear terms in the carrier phase equations. The linear terms are integrated with the implicit Crank-Nicolson method. The numerical model for the compressible carrier phase adopts explicit Runge-Kutta time-stepping and a second order finite volume discretization. Boundary conditions in the stream- and spanwise directions are periodic, while no-slip conditions are enforced at the walls. The domain has a size of $4\pi H$ in streamwise direction and $2\pi H$ in spanwise direction, where H is half the channel height. For the incompressible case the simulations were performed at a fixed value of the frictional Reynolds number, $\mathrm{Re}_\tau = 150$. In the compressible case the total flow rate was kept constant and from the simulation we found $\mathrm{Re}_\tau = 155.6$.

A constant heat flux is applied through the walls: positive through the upper wall and negative through the bottom wall in order to conserve the total energy of the system. As a consequence, the fluid temperature is nonuniform and a gradient of temperature develops across the channel. Consequently, the relative humidity will also be nonuniform and evaporation and condensation will take place near the warmer top wall and the colder bottom wall, respectively, because of the fluid-droplet coupling.

The right-hand sides of the droplet equations contain fluid properties at the droplet location. In order to determine these, tri-linear interpolation is applied. Droplets are assumed to collide elastically with the solid walls. Periodic conditions are applied for the droplets: if a droplet leaves the domain, it is reinserted at the opposite boundary with the same properties. To calculate the two-way coupling terms the sums in the expressions (13-15) are taken over all the droplets that are contained in a particular cell. At any time, a droplet contributes only to the flux corresponding to the grid cell it is contained in.

The incompressible and compressible formulations adopt different scales to arrive at the non-dimensional description. Hence, proper attention needs to be given to the initial condition. In both cases simulations are initialized using a statistically stationary turbulent velocity field obtained from a previous simulation without droplets. We distribute randomly 2,000,000 identical droplets with initial Stokes number $\mathrm{St} = 10$. In this way, the initial volume fraction is on the order of 10^{-4}, so that droplet-droplet collisions can be ignored but two-way coupling is relevant, Elghobashi (1994).

The initial temperature and vapor mass fraction are uniform for the incompressible model. The set-up of the initial condition for the compressible formulation needs more attention. If we compute the actual Mach number, based on the chosen reference scales, it has a value around 0.005. A Mach number this small leads to an extremely small time-step for the chosen numerical method. Rather than turning to an explicit low-Mach formulation, we adopt a low, but much higher value of 0.2. Corresponding to this much higher Mach number, noticeable variations in the initial temperature field arise on the order of 3 K. The initial mass density of the carrier phase was chosen from the condition of uniform relative humidity (RH), which is set equal to 100%. Velocity and temperature of the droplets are initialized using the fluid values at the random droplet location.

3 Comparison of compressible and incompressible simulations

In this section results obtained from the compressible and incompressible formulations will be compared. First, fluid flow properties will be compared, showing a close agreement between the two formulations. Then, we compare heat and mass transfer, which show larger differences.

Mechanical properties of the system

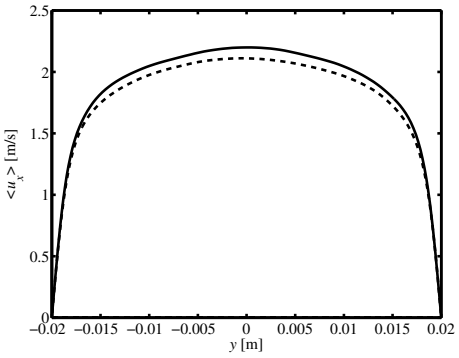

Figure 1: Streamwise fluid velocity averaged over the homogeneous directions at $t^+ = 2400$ as a function of the wall-normal coordinate: incompressible flow (solid) and compressible flow (dashed).

The velocity components of the carrier phase show good agreement between the two examined formulations. In Figure 1 the mean streamwise velocity component of the fluid is shown as a function of the wall-normal coordinate at a late time at which the flow has developed considerably. This level of agreement between the two formulations shows that the artificially large Mach number affects fluid flow aspects only to a small amount.

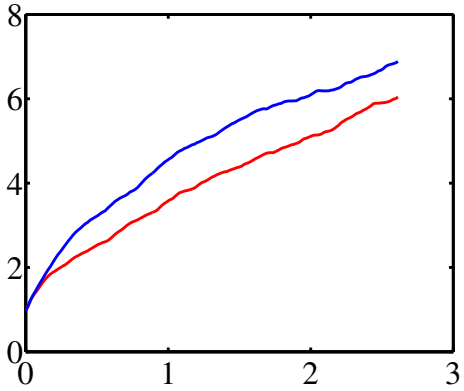

Figure 2: Droplet concentration near the hot wall as a function of time: incompressible flow (solid) and compressible flow (dashed).

The development of the concentration of the droplets is characterized by Figure 2. The concentration of the droplets near the hot wall increases with time, expressing the influence of turbophoresis (Kuerten, 2006). The tendency of the droplets to migrate toward the walls is similar in both formulations. In incompressible flow this tendency is stronger during the initial stages of the development of the flow. After about 1 s the rate with which the droplet concentration

grows is seen to be very similar for both models - the initial difference is likely to be due to the difference in the initial temperature profiles.

Heat transfer properties

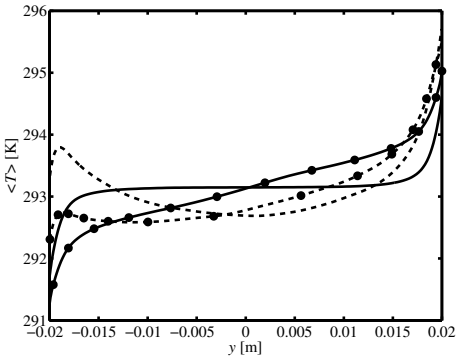

Figure 3: Fluid temperature averaged over the homogeneous directions as a function of the wall-normal coordinate. We show results at $t^+ = 160$ (no markers) and at $t^+ = 2400$ (with markers). Incompressible flow (solid) and compressible flow (dashed).

The mean temperature profile within the channel develops with time, as shown in Figure 3. We observe considerable differences in the mean temperature profiles. The solution at $t^+ = 160$ still contains a strong connection with the initial condition. The differences at a later time seem to be somewhat reduced, at least near the hot wall at $y = 0.02$ m. We observe an interesting asymmetric temperature profile, which is much stronger in the compressible formulation. Apart from differences due to the initial condition, the temperature profiles remain quite different at later times, also due to the non-physical value of the Mach number in the compressible simulation. We expect these differences to be strongly reduced when a proper low-Mach formulation is used.

To appreciate the development of the mean fluid temperature, we show the evolution of the value of T at the cold and hot walls with time in Figure 4. We observe that at both the hot and the cold wall the fluid temperature is slightly higher in case the compressible formulation is used. Moreover, the average temperature difference between the hot and the cold wall is slightly smaller in the compressible case. The rate at which the solution appears to approach the statistically steady state is quite similar for both formulations.

To express the efficiency of the heat transfer, it is common to investigate the Nusselt number. We define this quantity in the following way:

$$\mathrm{Nu} = \left(\frac{d\overline{T_g}}{dy} \bigg|_{wall} \right) \Big/ \frac{\Delta \overline{T_g}}{2H} \qquad (16)$$

where bars denote averaging over the two homogeneous directions, ΔT_g is the difference in gas temperature between the two walls and the derivative with

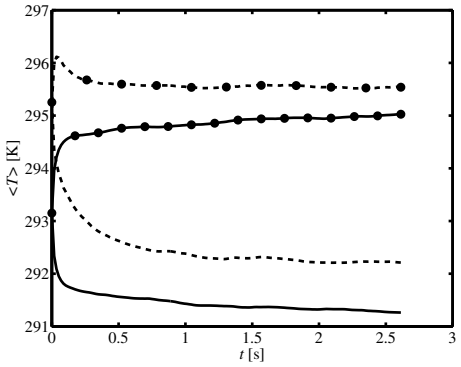

Figure 4: Fluid temperature at the cold and hot wall, averaged over the homogeneous directions as a function of time. Results for the cold wall (no marker) and the hot wall (with marker) are shown for the incompressible flow (solid) and compressible flow (dashed).

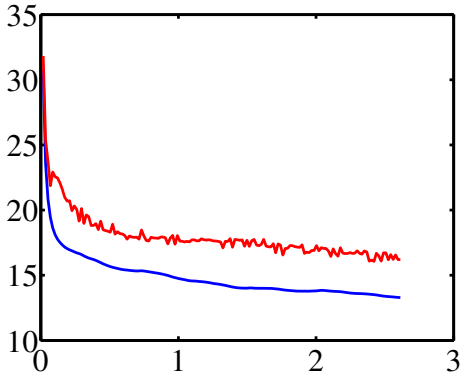

Figure 5: Nusselt number developing in time. Incompressible flow (solid) and compressible flow (dashed).

respect to the wall-normal coordinate in the numerator is the average over both walls. Figure 5 shows how the Nusselt number depends on time for both formulations. We observe a close agreement with a relative difference of about 25 %. The compressible formulation predicts a slightly higher value than the incompressible case. In the incompressible case Nu is about 20 % higher compared to the case without evaporation and condensation (Kuerten et al. 2011).

Droplets size

The comparison of the dispersed phase is made in terms of the nonuniform droplet size that develops across the channel. Figure 6 shows how the diameter of the droplets depends on the wall-normal coordinate at two characteristic times. The droplets at the walls behave very similarly in both cases: they condense at the cold wall, and evaporate near the hot wall. As can be seen, the transfer of mass is a more dynamic process in the compressible case. In the middle of the channel droplets are still very close to their initial size, when the incompressible formulation is used. In the

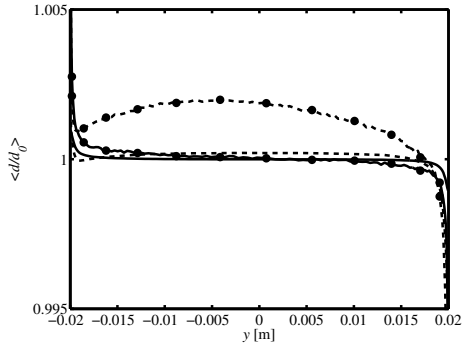

Figure 6: Normalized diameter of the droplets, averaged over the homogeneous directions, as a function of the wall-normal coordinate. Results at $t^+ = 160$ (no markers) and at $t^+ = 2400$ (with markers) are shown for incompressible flow (solid) and compressible flow (dashed).

compressible flow at late times, vapor appears to condense onto the droplets, leading to a slight increase in their average size. Referring back to the mean temperature profile of the carrier phase, cf. Figure 3, it can be seen that the mean temperature near the center of the channel is lower in the compressible case than in the incompressible case. Moreover, due to the initial non-uniform vapor mass fraction in the compressible case, vapor will diffuse toward the center of the channel. This explains the more intense condensation for the compressible formulation.

4 Concluding remarks

We compared an incompressible and a compressible formulation for particle-laden turbulent channel flow. The comparison involved two independently developed codes, adopting completely different spatial and temporal discretization methods. In general, good agreement for fluid flow and particle dispersion properties was found between these two formulations, establishing the correctness of the two numerical implementations. Heat and mass transfer are less similar. These differences have two main sources, i.e. the difference between the computational and the actual Mach number in the compressible formulation, which is also the reason for the different initial condition, and the inherent restriction of constant carrier gas mass density in the incompressible formulation.

During the initial stages of the developing flow the differences between the two formulations are obviously caused by the different initial fields. The compressible initial conditions show non-uniform temperature and vapor concentrations arising from the requirement of 100 % relative humidity. These are a direct consequence of the artificially high Mach number. Approaching the statistically steady state, these differences become smaller but still remain.

The main point of attention for future work regarding the compressible formulation will be to implement a low-Mach specific algorithm. This will allow a more physical comparison between the incompressible and compressible models. In this way the question whether the possibility of the compressible formulation to incorporate changes in carrier gas mass density is necessary for an accurate description of this flow can be answered. We plan to also investigate heated channel flows at much stronger thermal forcing, in which case compressibility effects certainly become more pronounced.

Acknowledgments

This work is supported through a PhD grant within the FOM DROP program and a PhD grant provided by the Dutch Technology Foundation STW, applied-science division of NWO (Netherlands Organisation for Scientific Research), and the Technology Program of the Ministry of Economic Affairs of the Netherlands. This work was sponsored by the Stichting Nationale Computerfaciliteiten (National Computing Facilities Foundation, NCF) for the use of supercomputer facilities, with Financial support from the Nederlandse Organisatie voor Wetenschappelijk Onderzoek, NWO.

References

Bird, R.B., Stewart, W.E. and Lightfoot, E.N. (1960), Transport phenomena, *John Wiley and Sons*

Elghobashi, S. (1994), On predicting particle-laden turbulent flows, *Applied scientific research*, Vol. 52, pp. 309–329

Kuerten, J.G.M. (2006), Subgrid modeling in particle-laden channel flow, *Phys. Fluids*, Vol. 18, 025108

Kuerten, J.G.M., Van der Geld, C.W.M. and Geurts, B.J. (2011), Turbulence modification and heat transfer enhancement by inertial particles in turbulent channel flow, *Phys. Fluids*, Vol. 23, 123301

Mashayek, F. (1997), Direct numerical simulations of evaporating droplet dispersion in forced low Mach number turbulence, *Int. J. Heat Mass Transfer*, Vol. 41, pp. 2601–2617

Maxey, M.R. and Riley, J.J. (1983), Equation of motion for a small rigid sphere in a nonuniform flow, *Phys. Fluids*, Vol. 26, pp. 883–889

Russo, E., Kuerten, J.G.M., Van der Geld, C.W.M. and Geurts, B.J. (2011), Modeling water droplet condensation and evaporation in DNS of turbulent channel flow, J. Phys.: Conference Series Vol. 318, 052019